

---

## ELASTIC $^{16}\text{O}+^{16}\text{O}$ SCATTERING AND NUCLEUS-NUCLEUS POTENTIAL WITH A REPULSIVE CORE

O.I. DAVIDOVSKAYA, V.YU. DENISOV

PACS 25.70.-z, 25.70.Bc  
©2010

Institute for Nuclear Research, Nat. Acad. of Sci. of Ukraine  
(47, Nauky Ave., Kyiv 03680, Ukraine)

---

Elastic  $^{16}\text{O}+^{16}\text{O}$  scattering at energies of 124, 145, 250, 350, and 480 MeV is analyzed in the framework of the optical model with the use of the nucleus-nucleus potential with a repulsive core. The elastic scattering cross-section is calculated with regard for the core and without it. It is shown that taking the core into account will result in an increase of the elastic scattering cross-section at backward angles. The decomposition of the scattering amplitude into the near- and far-side components is studied.

---

### 1. Introduction

Much attention is recently paid to the study of elastic scattering reactions of light and heavy ions. In order to analyze these reactions, one needs to know the nucleus-nucleus interaction potential that determines the elastic scattering cross-section [1–3]. The potential of nucleus-nucleus interaction consists of the nuclear, Coulomb, and centrifugal parts. The Coulomb and centrifugal interactions of two nuclei are well known. The nuclear part of the nucleus-nucleus interaction can be estimated, by employing various approaches: macroscopic, semimicroscopic, and microscopic ones [1–20].

The nuclear part of the interaction potential is often parametrized by the Woods–Saxon potential [1–3] or the double-folding potential [2–8]. These potentials are attractive at any distances between nuclei. In contrast, the proximity potential [9] or those based on the Skyrme forces [10–14] are attractive at large and close distances between interacting nuclei and are repulsive at very small distances, when nuclei are strongly overlapped. This repulsion is related to the high incompressibility coefficient of nuclear matter, the contribution made by the kinetic energy, the Pauli principle, and antisymmetrization [10–14].

A large amount of experimental data was analyzed with the Woods–Saxon potential or the double-folding potential [1–8]. However, very few reactions have been considered with the use of the potential with a repulsive core at small distances [10, 15–21]. Works [19–21] were devoted to the study of the elastic scattering reactions  $^{16}\text{O}+^{12}\text{C}$  and  $^{12}\text{C}+^{12}\text{C}$  in the framework of the optical model on the basis of the nucleus-nucleus potential with a repulsive core. The parameters of this potential were found by fitting the experimental data on elastic scattering. It is worth noting that the  $^{12}\text{C}$  and  $^{16}\text{O}$  nuclei are very stiff, that is why elastic scattering reactions with their participation are sensitive to the behavior of the potential at small nucleus-nucleus distances [7, 19–21]. The purpose of this work is to analyze the elastic scattering reaction  $^{16}\text{O}+^{16}\text{O}$  at various energies using the repulsive core potentials from [19–21].

### 2. Potential Parametrization

The real part of the nucleus-nucleus potential  $v(R)$  consists of the Coulomb  $v_C(R)$ , nuclear  $v_N(R)$ , and centrifugal  $v_l(R)$  components:

$$v(R) = v_C(R) + v_n(R) + v_l(R). \quad (1)$$

For the Coulomb and centrifugal components, we propose the following relations:

$$v_C(R) = \begin{cases} \frac{Z_1 Z_2 e^2}{R}, & R \geq R_C, \\ \frac{Z_1 Z_2 e^2}{R_C} \left[ \frac{3}{2} - \frac{R^2}{2R_C^2} \right], & R < R_C, \end{cases} \quad (2)$$

$$v_l(R) = \frac{\hbar^2 l(l+1)}{2M [A_1 A_2 / (A_1 + A_2)] R^2}. \quad (3)$$

Here,  $A_{1,2}$  and  $Z_{1,2}$  denote the numbers of nucleons and protons in the corresponding nuclei, respectively,  $e$  is the proton charge,  $M$  is the nucleon mass,  $R_C = r_C(A_1^{1/3} + A_2^{1/3})$ , and  $l$  is the orbital momentum.

The imaginary part of the nuclear potential consists of the volume and surface components

$$W(R) = -\frac{W_0}{1 + \exp[(R - r_w(A_1^{1/3} + A_2^{1/3}))/d_w]} - \frac{W_s \exp[(R - r_s(A_1^{1/3} + A_2^{1/3}))/d_s]}{d_s \{1 + \exp[(R - r_s(A_1^{1/3} + A_2^{1/3}))/d_s]\}^2}. \quad (4)$$

Such a representation of the imaginary part is common in the theory of nucleus-nucleus collisions [1-3].

### 2.1. Parametrization of the Nuclear Part of the Potential. Type A

First, we consider that the nuclear part of the potential can be parametrized in the form of a common long-range part parametrized by the Woods-Saxon potential and the short-range repulsive part of the core potential  $V_{\text{core}}(R)$

$$v_N(R) = \frac{-V_0}{1 + \exp[R - r_0(A_1^{1/3} + A_2^{1/3})/d_0]} + V_{\text{core}}(R). \quad (5)$$

Here, the core potential is determined in the same way as that in [19]:

$$V_{\text{core}}(R) = C_{\text{core}}v(R, a). \quad (6)$$

Here,

$$v(R, a) = \frac{4\pi a^3}{3} - \pi R a^2 + \frac{\pi R^3}{12} \quad (7)$$

for  $R < 2a$  and  $v(R \geq 2a, a) = 0$ , and  $C_{\text{core}}$  and  $a$  are the fitting parameters dependent on the collision energy.

Thus, we obtain 12 parameters of the potential belonging to its real and imaginary parts:  $V_0$ ,  $r_0$ ,  $d_0$ ,  $C_{\text{core}}$ ,  $a$ ,  $R_C$ ,  $W_w$ ,  $r_w$ ,  $d_w$ ,  $W_s$ ,  $r_s$ , and  $d_s$ .

### 2.2. Parametrization of the Nuclear Part of the Potential. Type B

Let us consider another parametrization of the nuclear part of the heavy-ion potential [20, 21],

$$v_N(R) = \begin{cases} \frac{-V_0}{1 + \exp[R - r_0(A_1^{1/3} + A_2^{1/3})/d_0]}, & R \geq R_m, \\ b_0 + b_1 s + b_2 s^2 + b_3 s^3 + b_4 s^4, & R < R_m, \end{cases} \quad (8)$$

where  $s = R - R_m$ . Since the nuclear part of the potential and its derivative are to be continuous at the matching point  $R_m$ , we obtain

$$b_0 = \frac{-V_0}{1 + \exp[(R_m - r_0(A_1^{1/3} + A_2^{1/3}))/d_0]}, \quad (9)$$

$$b_1 = \frac{V_0 \exp[(R_m - r_0(A_1^{1/3} + A_2^{1/3}))/d_0]}{d_0 \{1 + \exp[(R_m - r_0(A_1^{1/3} + A_2^{1/3}))/d_0]\}^2}. \quad (10)$$

So, the parametrization of type B is characterized by 14 parameters for the real and imaginary parts of the potential:  $V_0$ ,  $r_0$ ,  $d_0$ ,  $b_2$ ,  $b_3$ ,  $b_4$ ,  $R_m$ ,  $R_C$ ,  $W_w$ ,  $r_w$ ,  $d_w$ ,  $W_s$ ,  $r_s$ , and  $d_s$ .

Thus, deriving the parameters of the potential by fitting the experimental data on elastic scattering, one can describe the angular distribution of a nuclear reaction in the framework of the optical model.

## 3. Results and Discussion

### 3.1. Elastic Scattering

We obtain the parameters of the potential by fitting the data on elastic  $^{16}\text{O}+^{16}\text{O}$  scattering. For each collision energy, we find a set of parameters yielding the minimum value of  $\chi^2$ :

$$\chi^2 = \frac{1}{N} \sum_{i=1}^N \frac{(\sigma_{\text{calc}}(\theta_i) - \sigma_{\text{exp}}(\theta_i))^2}{(\delta\sigma_{\text{exp}}(\theta_i))^2}, \quad (11)$$

where  $N$  is the number of experimental points,  $\sigma_{\text{calc}}(\theta_i)$  and  $\sigma_{\text{exp}}(\theta_i)$  are the theoretical and experimental values of the cross-section at the angle  $\theta_i$ , correspondingly, and  $\delta\sigma_{\text{exp}}(\theta_i)$  is the corresponding error.

In order to increase the weight of the data at large angles, which are especially sensitive to the strength and the form of the optical potential at small distances, we assume (like [4, 5, 8, 19-21]) that  $\delta\sigma_{\text{exp}}(\theta_i) = 0.1\sigma_{\text{exp}}(\theta_i)$  for all data. The reaction  $^{16}\text{O}+^{16}\text{O}$  was considered at beam energies of 124, 145, 250, 350, and 480 MeV [8]. The obtained parameters of the potential are listed in Tables 1 (for the potential of type A) and 2 (for the potential of type B).

Figures 1-5 show the experimental data on elastic scattering for the  $^{16}\text{O}+^{16}\text{O}$  system at beam energies of 124, 145, 250, 350, and 480 MeV, as well as the results of fitting in the framework of the optical model for the potential with a repulsive core of type A. For comparison, Figs. 6-10 present similar calculations for the  $^{16}\text{O}+^{16}\text{O}$

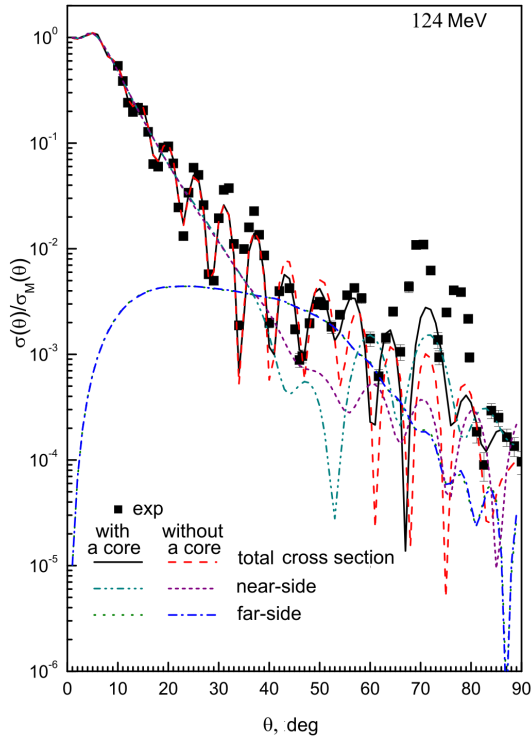


Fig. 1. Data on elastic  $^{16}\text{O}+^{16}\text{O}$  scattering and calculations by the optical model with the use of the nucleus-nucleus potential with a repulsive core of type A for a beam energy of 124 MeV

reaction at the same beam energies but for the potential with a repulsive core of type B.

**T a b l e 1.** Parameters of the optical potential of type A for the  $^{16}\text{O}+^{16}\text{O}$  system

$E_{\text{lab}}$ (MeV)	124	145	250	350	480
$E_{\text{lab}}$ (MeV)	124	145	250	350	480
$V_0$ (MeV)	28.246	28.503	28.729	29.602	28.902
$r_0$ (fm)	1.228	1.233	1.199	1.198	1.187
$d_0$ (fm)	0.611	0.574	0.460	0.489	0.462
$a$ (fm)	2.411	2.655	2.505	2.002	1.616
$C_{\text{core}}$ (MeV fm $^{-3}$ )	8.599	2.683	2.713	0.483	1.681
$R_C$ (fm)	6.159	6.175	6.692	6.972	6.999
$W_w$ (MeV)	14.659	13.355	5.071	5.000	7.077
$r_w$ (fm)	1.128	1.081	1.146	1.186	1.043
$d_w$ (fm)	0.179	0.135	0.243	0.234	0.241
$W_s$ (MeV)	15.047	16.425	18.057	14.803	17.937
$r_s$ (fm)	1.228	1.212	1.363	1.366	1.327
$d_s$ (fm)	0.781	0.717	0.857	0.899	0.867
$\sigma^a$ (mb)	1736	1671	2049	1954	1892
$\chi^2$	16.9	17.8	10.85	5.88	6.15

<sup>a</sup> The total reaction cross-section.

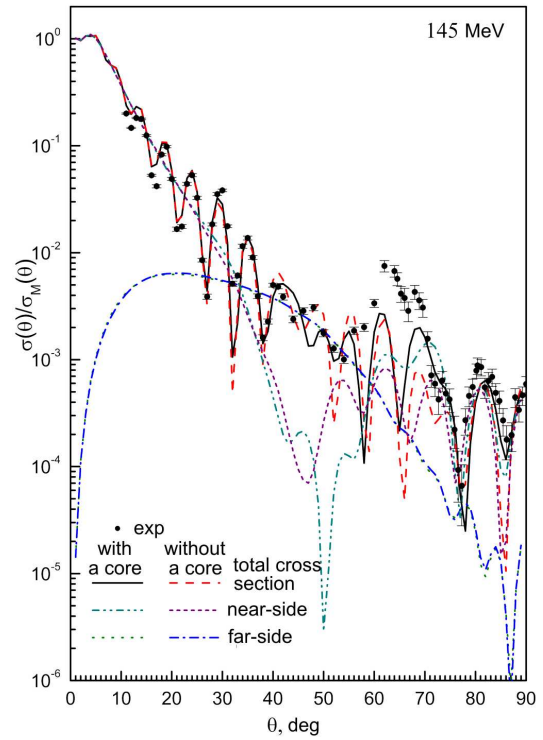


Fig. 2. The same as in Fig. 1 for a beam energy of 145 MeV.

In order to demonstrate the effect of the repulsive core, Figs. 1–10 show both the results of calculations according to the optical model for the potential with a repulsive core (solid curve) and without it (dotted

**T a b l e 2.** Parameters of the optical potential of type B for the  $^{16}\text{O}+^{16}\text{O}$  system

$E_{\text{lab}}$ (MeV)	124	145	250	350	480
$V_0$ (MeV)	30.263	43.659	36.945	35.926	44.436
$r_0$ (fm)	1.191	1.089	1.120	1.149	1.064
$d_0$ (fm)	0.757	0.742	0.677	0.513	0.682
$b_2$ (MeV fm $^{-2}$ )	2.671	6.353	5.316	5.888	0.116
$b_3$ (MeV fm $^{-3}$ )	5.547	6.609	5.527	7.229	4.984
$b_4$ (MeV fm $^{-4}$ )	1.234	1.149	0.999	1.268	1.022
$R_m$ (fm)	6.685	6.835	5.827	6.694	5.738
$R_C$ (fm)	6.357	6.532	6.370	5.395	7.794
$W_w$ (MeV)	15.406	13.229	11.916	32.855	17.896
$r_w$ (fm)	1.027	1.050	1.296	1.168	0.962
$d_w$ (fm)	0.159	0.251	0.730	0.549	0.4014
$W_s$ (MeV)	11.687	11.712	0.030	6.249	25.462
$r_s$ (fm)	1.305	1.251	1.240	1.337	1.072
$d_s$ (fm)	0.430	0.484	0.035	0.378	0.671
$\sigma^a$ (mb)	1606	1555	1677	1507	1500
$\chi^2$	11.01	14.42	7.86	7.79	5.66

<sup>a</sup> The total reaction cross-section.

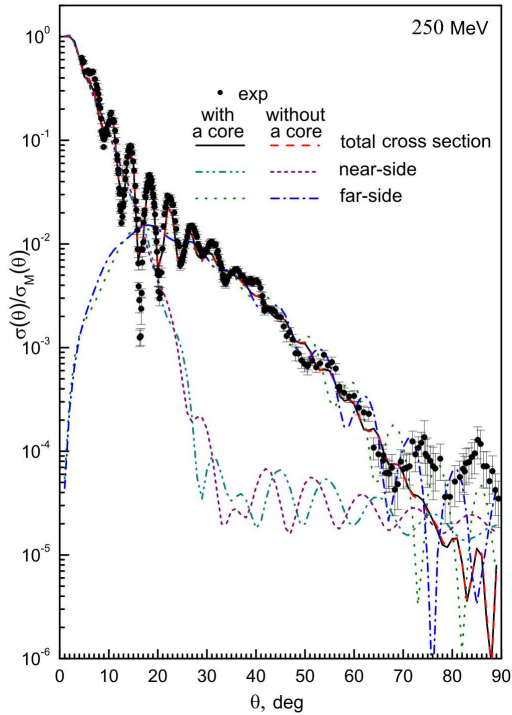


Fig. 3. The same as in Fig. 1 for a beam energy of 250 MeV

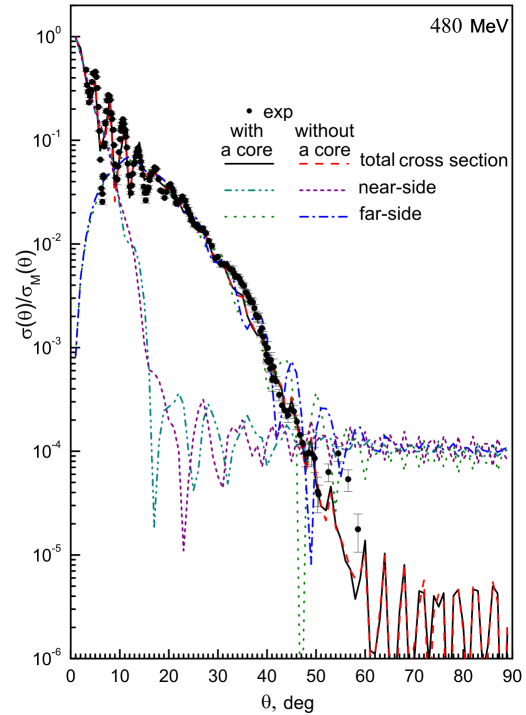


Fig. 5. The same as in Fig. 1 for a beam energy of 480 MeV

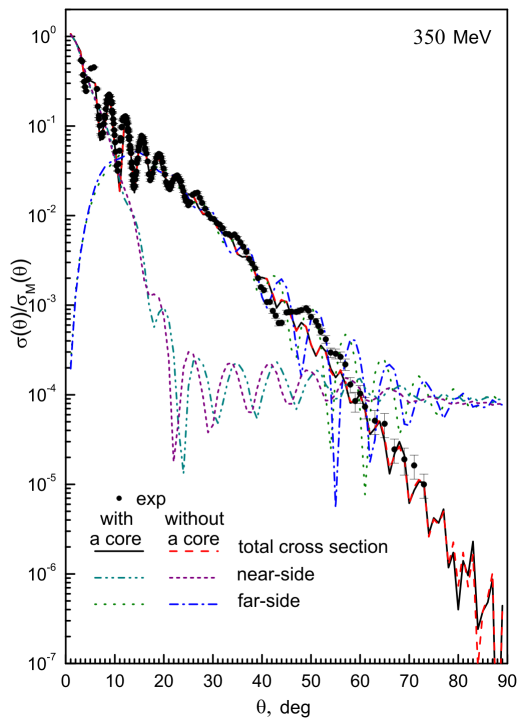


Fig. 4. The same as in Fig.1 for a beam energy of 350 MeV

curve). In this case,  $V_{\text{core}}(R) = 0$  for the potential of type A. The potential of type B without a core coincides with the corresponding potential with a repulsive core at the distances  $R \geq R_{\text{well}}$  and equals  $V_{\text{well}}$  at  $R < R_{\text{well}}$  ( $V_{\text{well}}$  is the minimum depth of the potential and  $R_{\text{well}}$  is the distance corresponding to the minimum potential). Comparing the results for elastic scattering given in Figs. 1–10, one can clearly see the effect of the repulsive core. Due to the inner repulsion, the elastic scattering cross-section considerably increases at backward angles. At forward angles, values of the cross-section are practically the same for the potentials with a repulsive core and without it for the both types of parametrization.

The total cross-sections of the reaction  $^{16}\text{O} + ^{16}\text{O}$  given in Tables 1, 2 are close to the corresponding values from [8]. However, the total cross-sections found for the parametrization of type A have larger values than those calculated for the parametrization of type B. The inner core does not influence the total cross-sections of the reaction.

The values of  $\chi^2$  obtained for the repulsive core potential (see Tables 1, 2) are close to the corresponding results obtained in [8]. Thus, the qualities of our description and that used in [8] are similar.

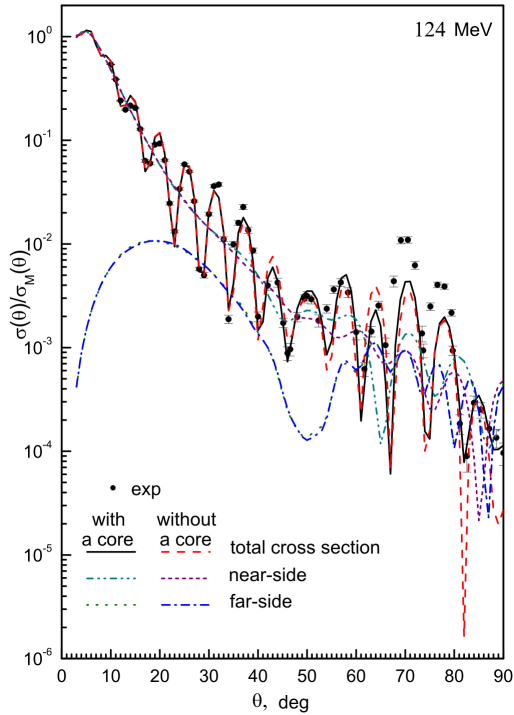


Fig. 6. Data on elastic  $^{16}\text{O}+^{16}\text{O}$  scattering and calculations by the optical model with the use of the nucleus-nucleus potential with a repulsive core of type B for a beam energy of 124 MeV

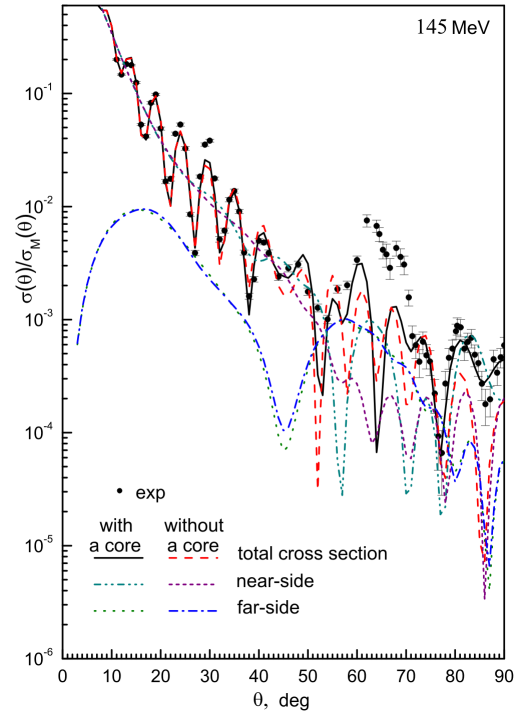


Fig. 7. The same as in Fig. 6 for a beam energy of 145 MeV

### 3.2. Potential

The real parts of the nucleus-nucleus potentials with a repulsive core (1)–(10) for  $l=0$  with the parameters from Tables 1 and 2 at various collision energies are presented in Fig. 11,*a* (for the potential of type A) and Fig. 11,*b* (for the potential of type B). The repulsive core potential has a core at small distances and a well at medium distances between nuclei, see Fig. 11. For comparison, this figure also shows the proximity [9] and semimicroscopic [12] potentials. The depth of the well depends on the collision energy for the repulsive core potential.

The minimum of the well evaluated at various collision energies lies at  $R \approx 4 \div 5$  fm for the potential of type A and at  $R \approx 2 \div 3.5$  fm for the potential of type B. As a rule, the repulsive core lies at the distances  $R \leq 2$  fm for any of the potentials presented in Fig. 11. Thus, the distance, where the densities of colliding nuclei are considerably overlapped and, hence, the incompressibility of nuclear matter and the Pauli principle result in the strong repulsion, is approximately the same for all potentials. The depth of the potentials obtained in [8] for various energies belongs to the interval between 282 and 452 MeV. As compared with these data, the repulsive

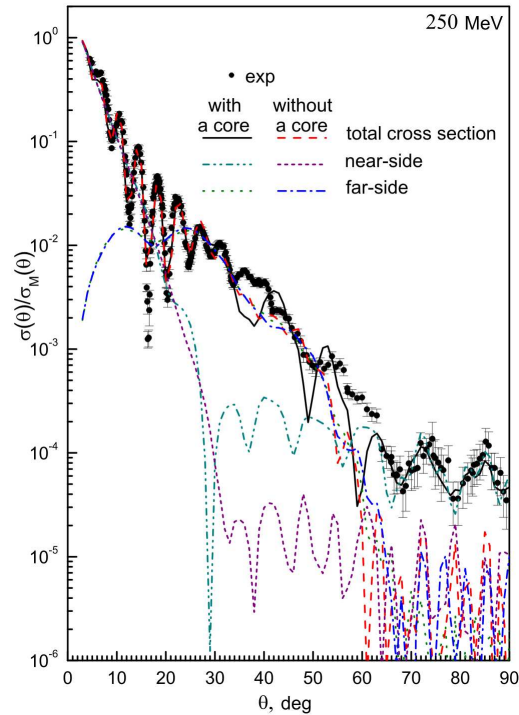


Fig. 8. The same as in Fig. 6 for a beam energy of 250 MeV

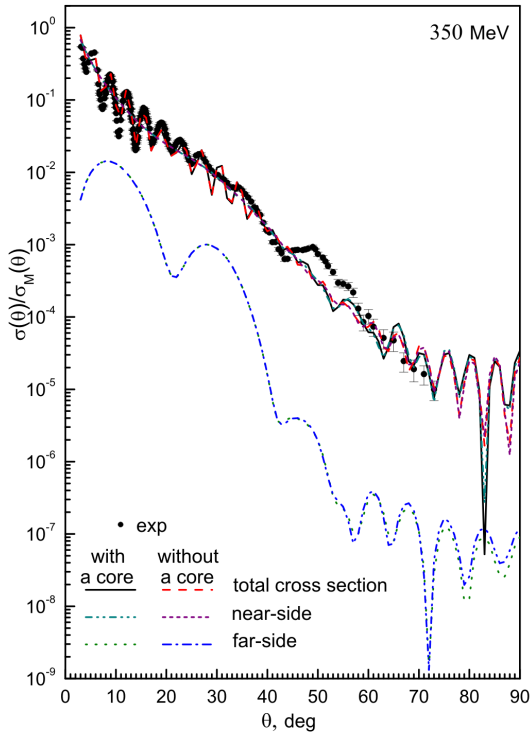


Fig. 9. The same as in Fig. 6 for a beam energy of 350 MeV

core potentials we have proposed are shallow (see Fig. 11).

It is worth noting that, for the parametrization of type A, the magnitude of the core essentially decreases, as the collision energy increases, in the same way as that for the reaction  $^{16}\text{O}+^{12}\text{C}$  [19–21]. However, for the  $^{16}\text{O}+^{16}\text{O}$  reaction, the form of the potential considerably changes at high energies for the both types of parametrization. It is possibly due to the fact that, at very high collision energies, nucleons in nuclei easily pass to vacant excited levels, which results in a decrease of the role of the Pauli principle and the contribution of the nucleon antisymmetrization to a magnitude of the core.

### 3.3. Near- and Far-Side Components of the Cross-Section

Employing the Fuller method [22], we obtained the near- and far-side components of the decomposition of the scattering amplitude for the  $^{16}\text{O}+^{16}\text{O}$  reaction using the potential with a repulsive core and without it (see Figs. 1–10). In [8], it was shown that the elastic scattering cross-section for this reaction is determined by the near-side component at forward angles and by the far-side component at backward angles. In this case, the far-

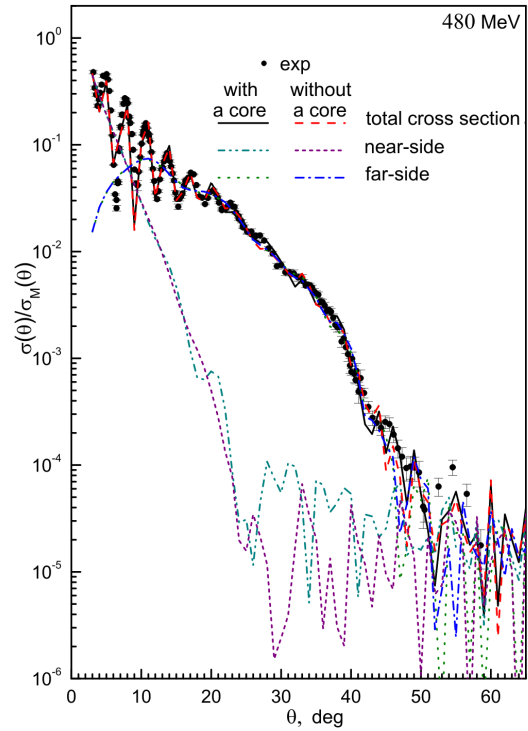


Fig. 10. The same as in Fig. 6 for a beam energy of 480 MeV

side component is related to the rainbow phenomenon [4–8] caused by the refraction of an incident wave due to the strongly attractive (very deep) nucleus-nucleus potential.

In our case, the near-side component for the potential of type A is important at forward and backward angles, and the far-side one — at medium angles (see Figs. 1–10). For the potential of type B, the near-side component mainly describes the cross-section in the full range of angles at energies of 124, 145, and 350 MeV, while the far-side component is important at backward angles and is responsible for the structure of oscillations caused by the interference of the near- and far-side components. At energies of 250 and 480 MeV, the near-side component is important at forward and backward angles, and the far-side one — at medium and backward angles. Due to the repulsive core, the near- and far-side components rise at backward angles.

We have also performed calculations with the help of the modified Fuller method [23] that eliminates nonphysical contributions to the near- and far-side components of the decomposition of the scattering amplitude. However, the influence of nonphysical contributions is inessential for the considered potential parametrizations.

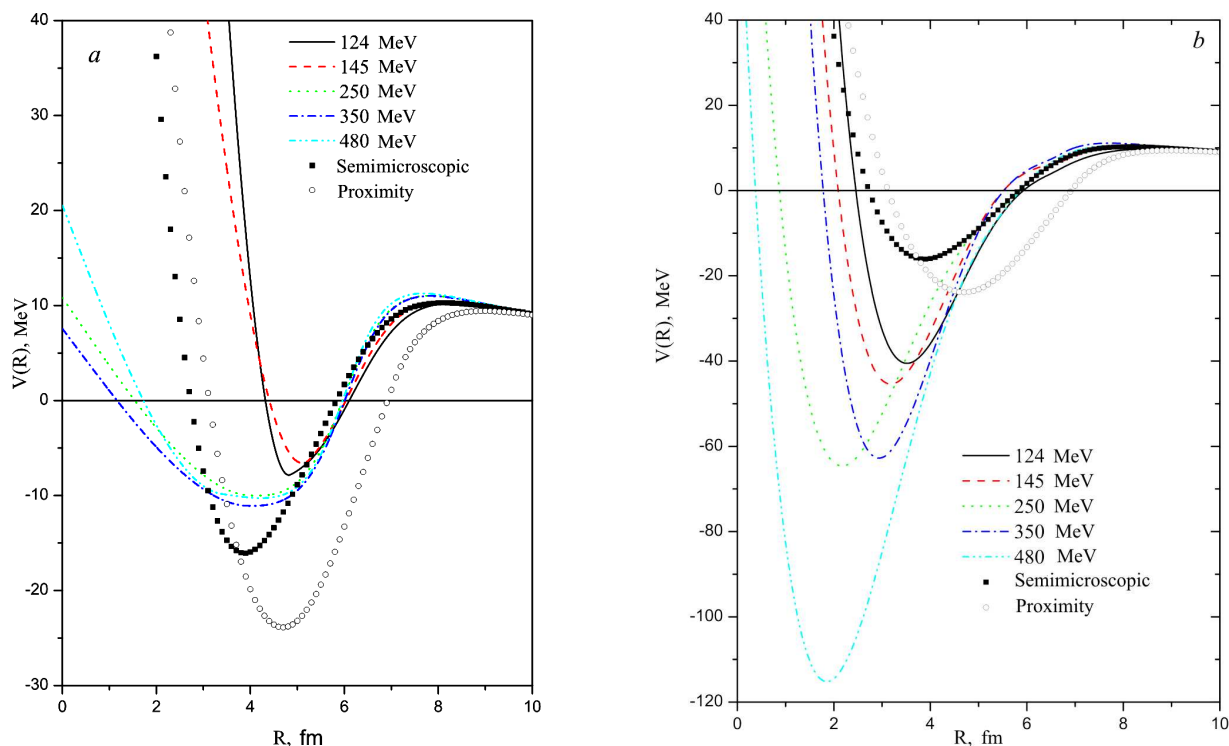


Fig. 11. Repulsive core potential determined for elastic  $^{16}\text{O}+^{16}\text{O}$  scattering at various beam energies: *a* – potential of type A; *b* – potential of type B. The proximity [9] (circles) and semimicroscopic [12] (squares) potentials are also given for comparison

#### 4. Conclusions

It is shown that the data on elastic  $^{16}\text{O}+^{16}\text{O}$  scattering can be described, by employing the shallow phenomenological potential with a repulsive core. We propose two different parametrizations of the nuclear part of the repulsive core potential with similar accuracies of description of the reaction cross-section. Due to the repulsive core, the cross-sections and the near- and far-side components of the scattering amplitude rise at backward angles. However, the total cross-section of the reaction does not depend on the core.

1. P.E. Hodgson, *Nuclear Heavy-Ion Reactions* (Clarendon Press, Oxford, 1978).
2. G.R. Satchler, *Direct Nuclear Reactions* (Oxford University, Oxford, 1983).
3. P. Frobrich and R. Lipperheide, *Theory of Nuclear Reactions* (Clarendon Press, Oxford, 1996).
4. A.A. Ogloblin, Dao T. Khoa, Y. Kondo, Yu.A. Glukhov, A.S. Dem'yanova, M.V. Rozhkov, G.R. Satchler, and S.A. Goncharov, *Phys. Rev. C* **57**, 1797 (1998).
5. A.A. Ogloblin, Yu.A. Glukhov, W.H. Trzaska, A.S. Dem'yanova, S.A. Goncharov, R. Julin, S.V. Klebnikov, M. Mutterer, M.V. Rozhkov, V.P. Rudakov, G.P. Tiorin, Dao T. Khoa, and G.R. Satchler, *Phys. Rev. C* **62**, 044601 (2000).
6. V.B. Soubbotin, W. von Oertzen, X. Vinas, K.A. Gridnev, and H.G. Bohlen, *Phys. Rev. C* **64**, 014601 (2001).
7. M.E. Brandan and G.R. Satchler, *Phys. Rep.* **285**, 143 (1997); Dao T. Khoa, W. von Oertzen, H.G. Bohlen, and S. Ohkubo, *J. Phys. G* **34**, R111 (2007); M.E. Brandan, *Phys. Rev. Lett.* **60**, 784 (1988).
8. Dao T. Khoa, W. von Oertzen, H.G. Bohlen, and F. Nuoffer, *Nucl. Phys. A* **672**, 387 (2000).
9. J. Blocki, J. Randrup, W.J. Swiatecki, and C.F. Tsang, *Ann. Phys. (N.Y.)* **105**, 427 (1977).
10. K.A. Brueckner, J.R. Buchler, and M.M. Kelly, *Phys. Rev.* **173**, 944 (1969).
11. F. Stancu and D.M. Brink, *Nucl. Phys. A* **270**, 236 (1976).
12. V.Yu. Denisov, *Phys. Lett. B* **526**, 315 (2002).
13. V.Yu. Denisov and W. Nörenberg, *Eur. Phys. J. A* **15**, 375 (2002).

14. V.Yu. Denisov and V.A. Nesterov, Phys. At. Nucl. **69**, 1472 (2006).
15. S. Misticu and H. Esbensen, Phys. Rev. C **75**, 034606 (2007).
16. T. Izumoto, S. Krewald, and A. Faessler, Nucl. Phys. A **341**, 319 (1980).
17. S. Hossain, M.N.A. Abdullah, K.M. Hasan, M. Asaduzzaman, M.A.R. Akanda, S.K. Das, A.S.B. Tariq, M.A. Uddin, A.K. Basak, S. Ali, and F.B. Malik, Phys. Lett. B **636**, 248 (2006).
18. K. A. Gridnev, E. E. Rodionova, and S. N. Fadeev, Yad. Fiz. **71**, 1290 (2008).
19. V.Yu. Denisov and O.I. Davidovskaya, Yad. Fiz. **73**, 429 (2010).
20. V. Yu. Denisov and O.I. Davidovskaya, Ukr. Fiz. Zh. **54**, 669 (2009).
21. V.Yu. Denisov and O.I. Davidovskaya, Izv. RAN. Ser. Fiz. **74**, 611 (2010).
22. R.C. Fuller, Phys. Rev. C **12**, 1561 (1975).
23. Yu.A. Bereznoi and V.V. Pilipenko, Izv. RAN. Ser. Fiz. **59**, 197 (1995).

Received 02.02.10

Translated from Ukrainian by H.G. Kalyuzhna

ПРУЖНЕ РОЗСІЯННЯ  $^{16}\text{O}+^{16}\text{O}$  І ЯДЕРНО-ЯДЕРНИЙ ПОТЕНЦІАЛ ІЗ ВІДШТОВХУВАЛЬНИМ КОРОМ*О.І. Давидовська, В.Ю. Денисов*

## Резюме

Пружне розсіяння  $^{16}\text{O} + ^{16}\text{O}$  при енергіях 124, 145, 250, 350, 480 MeV проаналізовано в рамках оптичної моделі з використанням ядерно-ядерного потенціалу з відштовхувальним кором. Виконано розрахунки для перерізу пружного розсіяння з урахуванням і без урахування кору. Показано, що врахування кору приведе до збільшення перерізу пружного розсіяння на задніх кутах. Досліджено розклад амплітуди розсіяння на ближню і дальню компоненти.